Geo-Marine Letters
https://doi.org/10.1007/s00367-019-00591-1

ORIGINAL

The role of frequency spread on swash dynamics

Jennifer Montaño[1,2] · Brice Blossier[3] · Andres F. Osorio[2] · Christian Winter[4]

Received: 26 December 2018 / Accepted: 26 August 2019

Abstract

The swash zone is the most dynamic part of the upper beach. Here breaking waves interact with sediments, leading to beach morphodynamics, and eventually to coastal erosion and flooding. An understanding of swash characteristics such as the vertical excursion and mean swash period is of vital importance to identify and predict the possible impact of storms in coastal areas. The prediction of these swash parameters is commonly based on bulk offshore spectral wave parameters and the beach slope, the latter being expensive to monitor. In this study, a dataset from an intermediate beach on the south-west coast of Sylt, Germany was derived to analyze swash characteristics. Field observations show high variability in swash excursion even for similar incident wave conditions if expressed by bulk parameters. Here, the role of frequency spread was further investigated. An inverse relationship between swash frequency spread and swash characteristics (excursion and mean period) was identified. A parameterization for the swash frequency spread based on incident wave parameters is proposed, and a new approach to obtain total swash excursion and mean swash period is developed. The parameterization is validated using two independent swash datasets (Duck 1982 and Duck 1994) and compared to the predictive ability of other parameterizations. It is highlighted that common parameterizations based on peak period do not perform well in characterizing incident conditions when bi-modal spectra are present. The choice of the right descriptor for wave periods may have a more pronounced influence on the predictive skill than the inclusion of the beach slope.

Introduction

The swash zone is the most dynamic part of the upper beach in which broken waves and infragravity waves uprush and downwash between the surf zone and the dry back beach. Swash zone dynamics have a strong impact on beach face morphology, longshore sediment transport, overtopping, and overwash. Therefore, the understanding of the processes within this zone is of vital importance for coastal management and for the prediction of beach dynamics, the planning of beach nourishments, or other coastal defense strategies (e.g., Sallenger 2000).

Swash zone processes are highly non-linear, and to date, system understanding is mainly based on empirical knowledge (Puleo and Torres-Freyermuth 2016). Research is driven to derive reliable parameterizations of run-up, defined as a (quasi) steady super-elevation of the mean water level (setup - $<\eta>$), and time-varying fluctuations around this super-elevation (swash, S) (Stockdon et al. 2006). Broken wave motions can be differentiated into (1) swash resulting from the collapse of high-frequency sea wind and swell waves ($f > 0.05$ Hz) and (2) swash resulting from low-frequency infragravity waves ($f < 0.05$ Hz).

Commonly, run-up is predicted from offshore bulk parameters such as the wave height H_0 and wavelength $L_0 = {}^{gT_0^2}/_{2\pi}$, where T_0 is the wave period and the beach slope β (e.g., Holman and Sallenger 1985; Stockdon et al. 2006; Senechal et al. 2011; Gomes da Silva et al. 2018). Other studies have introduced additional parameters: Polidoro et al. 2013 improved run-up

✉ Jennifer Montaño
jmon177@aucklanduni.ac.nz

1 School of Environment, Faculty of Science, University of Auckland, Auckland 1142, New Zealand

2 Sede Medellín-Facultad de Minas-Departamento de Geociencias y Medio Ambiente, Grupo de Investigación OCEANICOS, Universidad Nacional de Colombia, Cr. 80 # 65 -223, M2, 209 Medellín, Colombia

3 MARUM, Center for Marine Environmental Sciences, University of Bremen, Leobener Str. 8, 28359 Bremen, Germany

4 Christian-Albrechts-Universität zu Kiel-Institute of Geosciences, Otto-Hahn-Platz 1, 24118 Kiel, Germany

Published online: 14 November 2019

parameterizations on gravel beaches, including the incident spectral peakedness parameter Q_p, to take into account bimodal wave spectra which are very common on the southeast coast of England. Using a numerical model, Guza and Feddersen (2012) found that including the frequency spread offshore $f_{s,0}$ and directional spread σ_θ on run-up parameterizations at the infragravity band reduced the scatter on run-up predictions. The influence of nearshore morphology (such as surf/swash zone interactions) and longshore variability (e.g., the presence of beach cusps) have been identified to also play an important role in swash excursion dynamics (Masselink and Puleo 2006; Bryan and Coco 2010; Senechal et al. 2018; Almar et al. 2018). Other parameters, such as the tidal stage (Guedes et al. 2011; Almar et al. 2016; Medellín et al. 2016) and wave groupness (Baldock and Holmes 1999; Roelvink et al. 2018) were found to be relevant especially at the infragravity band. Also, smaller scales related with near-bed dynamics such as grain size (Poate et al. 2016), beach variability (Cohn and Ruggiero 2016; Senechal et al. 2018), swash-swash interactions, and the role of infiltration and exfiltration have been also addressed (e.g., Masselink and Puleo 2006; Brocchini and Baldock 2008).

As with run-up prediction, many studies have also been devoted to understanding and predicting the spectral shape of the swash spectra, focusing on the energy roll-off, where short waves are saturated due to wave breaking. This saturation slope has been found to be proportional to f^{-4} (intermediate-reflective beaches) or f^{-3} (dissipative beaches), where f is the frequency (e.g., Guza and Thornton 1982; Guedes et al. 2013; Ruju et al. 2013; Hughes et al. 2014; Peláez-Zapata et al. 2018). Certain statistical parameters such as the spectral width, frequency spread, or peakedness have been used to describe the energy distribution (spectral shape) offshore (Cartwright and Longuet-Higgins 1956; Longuet-Higgins 1983; Goda 1970). However, these parameters have been neglected in the study of swash spectral features. The purpose of this paper is to discuss the influence of energy distribution in the swash spectra (through the frequency spread f_s parameter) on swash dynamics. We derived and analyzed a dataset from an intermediate beach on the south-west coast of Sylt island, Germany (Fig. 1), observing a clear inverse relationship between the total swash excursion (S) and mean swash period ($T_{02,s}$) and the swash frequency spread ($f_{s,s}$). A parameterization of the frequency spread in the swash zone $f_{s,s}$ based on incident wave parameters is proposed. A new approach to calculate the total swash excursion and mean swash period is derived in data from Sylt, taking into account the swash frequency spread based on incident wave parameters. A simplification of the total swash excursion parameterization is then tested on two independent datasets (Duck 1982 and Duck 1994). Finally, the influence of the different wave periods and beach slope on the predictions is assessed.

Methods

Study area

The present study was carried out at Bunkerhill Beach, Sylt island, one of the North Frisian barrier islands located in the German Bight, in the North Sea (Fig. 1). Bunkerhill Beach is a steep sloping sandy beach (medium to coarse sand) which generally exhibits a double-barred profile with semi-diurnal tides ranging around 2 m (Blossier et al. 2017). Waves are generated from westerly winds, mainly between 245 and 315°, with the highest waves coming from the North West. For the time period 2013–2017, mean significant wave heights recorded by the offshore buoy Westerland fluctuate around 1 m. Maximum significant wave heights can exceed 5 m, with wave periods generally between 3 and 8 s (BSH 2019).

Beach topography is surveyed by the relevant authorities (Landesbetrieb für Küstenschutz, Nationalpark und Meeresschutz Schleswig-Holstein) with airborne lidar and RTK-GPS. Figure 1 b shows beach profiles at different times from 2013 to 2015. The shore-face slope, − 0.5–2 m above MSL (gray square, Fig. 1b), was similar during the different measurement periods. Values were between 0.11 and 0.16, with most of them around 0.13.

Data acquisition and analysis

The incident wave spectra were obtained from a wave buoy (operated by the Helmholtz Zentrum Geesthacht HZG) located seaward of the subtidal bar crest at a depth of approximately 7 m (Fig. 1). Swash zone information was acquired through a video monitoring system installed at Bunkerhill Beach. The camera is mounted on top of a measuring station 25 m above MSL. High-resolution images (2016 × 1528 pixels) were collected every hour during daylight conditions, at a sampling frequency of 4 Hz for 20 min. This study used camera data from October to December 2014 and June 2015. Swash excursion was extracted from "time-stack" images (Aagaard and Holm 1989), i.e., the pixel intensity time series along a specific cross-shore transect (Fig. 1c). To process the swash time series, an algorithm was developed that detects the wet-dry interface on the beach by using the maximum contrast between the swash front (white foam) and sand (Fig. 2 upper panels). A visual inspection was then performed, and manual corrections were applied where necessary. Ground control points were implemented to transform the pixel coordinates into real-world coordinates, and the resulting profile was projected onto a cross-shore transect, perpendicular to the average beach orientation (Fig. 2, bottom panels).

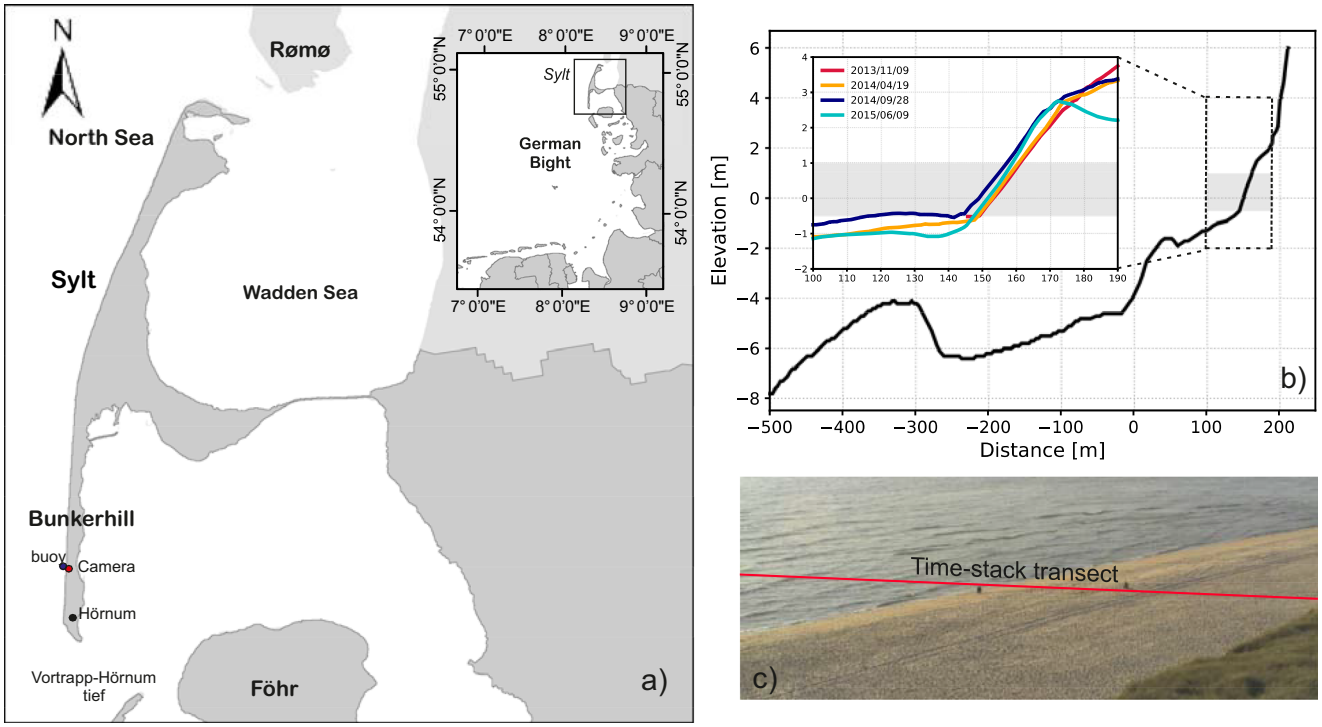

Fig. 1 **a** Location of Bunkerhill Beach, Sylt (Germany). Camera system (red dot) and wave buoy (blue dot). **b** Beach profile showing double bar (black line). Panel **b** also displays a magnified view of the beach profiles in the upper part of the beach at different times from 2013 to 2015 (colors). The gray shadow in panel **b** represents the part of the beach where time-stacks were analyzed (− 0.5–1 m above MSL). **c** The red line is the time-stack transect used to obtain swash time-series

Different statistical parameters have been used to describe the spectral shape (energy distribution): Cartwright and Longuet-Higgins (1956) proposed the spectral width parameter $\varepsilon = \left(1-\frac{m_2^2}{m_0 m_4}\right)^{0.5}$, with $\varepsilon \to 0$ when energy is concentrated within a narrow band and $\varepsilon \to 1$ when energy is spread over a broader band. Here m_n corresponds to the n spectral moment. To calculate the moments, the highest cut off frequency was 0.5 Hz, since the high-order moments are sensitive to noise (Holthuijsen 2008), whereas the lowest cut off frequency was 0.003 Hz. Later, Longuet-Higgins (1983) gave an alternative parameter to measure the narrowness of the spectrum, defined as $\nu = \left(\frac{m_0 m_2}{m_1^2}-1\right)^{0.5}$. Another spectral shape parameter is the spectral peakedness $Q_p = \frac{2}{m_0^2}\int_0^\infty f[S(f)]^2 \mathrm{df}$, which is related to the spectral width parameter ε (Goda 1970). These parameters were calculated to evaluate the energy distribution of the swash spectra. In our case, the frequency spread parameter $f_s = \left(\frac{m_2}{m_0}-\frac{m_1^2}{m_0^2}\right)^{0.5}$ was used as it correlated well with the swash excursion. High values of the frequency spread represent wide spectra and vice-versa.

Commonly, the peak period T_p is used in run-up predictions. However, for bimodal wave spectra, the use of this parameter may not be appropriate to describe incident wave conditions (Van der Meer and Janssen 1994; Polidoro et al. 2013; Poate et al. 2016). Therefore, T_p may also fail as a descriptor for the swash zone as the spectra may be multimodal or very broad. Since broad and bimodal incident conditions were observed at Sylt beach, different parameterizations of wave periods could be tested, such as the spectral mean wave period $T_{-1,0} = {}^{m_{-1}}/_{m_0}$, the mean spectral period $T_{0,1} = {}^{m_0}/_{m_1}$, and the mean period $T_{0,2} = \left({}^{m_0}/_{m_2}\right)^{0.5}$. In addition, bimodality was analyzed following Poate et al. 2016, using the relationship $T_{-1,0}/T_{0,1}$, where values >~1.15 should represent bimodal sea states (in our case values >~1.2).

Although photographic images are available quasi-continuously, and spectral information described above can be calculated without further processing, the exact quantification of run-up heights can only be derived if the beach topography is known. The georeferenced image pixels can then be assigned to an exact vertical level. Topographic surveys were available for Sep 28, 2014 and Jun 9, 2015, allowing run-up to be calculated for 56 time-series from Sep 28, to Oct 4, 2014 and from Jun 4 to 10, 2015, as weather conditions were fair during those periods and no significant changes in the beach profile are expected.

For time periods for which no topographic surveys are available, the cross-shore transect can be defined by pixel coordinates only. The main consequence is that without knowing the topography, vertical swash excursion $\left(S = 4\sqrt{\int_{f_0}^{f_1} E(f)\mathrm{df}}\right)$ cannot be quantified in meters.

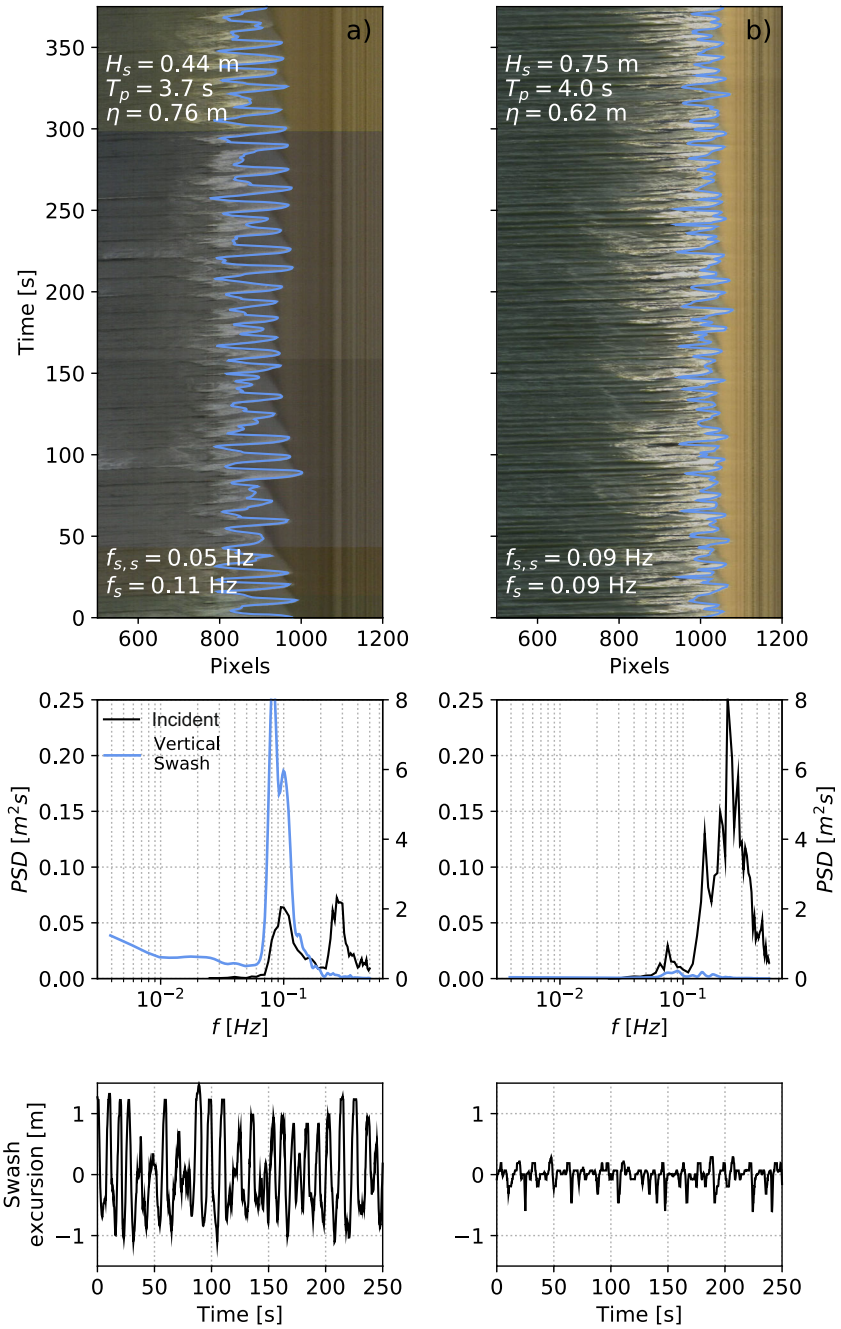

Fig. 2 Incident wave conditions and swash data at Bunkerhill beach for **a** September 30, 2014 at 17:30 and **b** June 10, 2015 at 18:30. Top panels: Examples of time-stack images and swash detection, incident wave height and period (H_s, T_p), tidal stage (η), swash frequency spread ($f_{s,\,s}$), incident frequency spread (f_s). Middle panels: Incident wave spectra (black lines, left axis) and swash spectra from the total swash excursion (blue line, right axis). Note that swash energy on June 10, 2015 is very low compared to that on September 30, 2014 at 17:30. Bottom panels: time-series of the detrended swash excursion

However, the spectral shape of swash data is similar which was tested for 56 time-series (where the topography was available). This is shown in Fig. 3c and d for the swash frequency spread $f_{s,s}$ and the mean swash period $T_{02,s}$, with a goodness of fit of $R^2 = 0.94$ and $R^2 = 0.97$, respectively. Therefore, 128 additional pixel intensity time-stacks, corresponding to August, October, and December of 2014 could be considered for the analysis. Only data at times with water levels between -0.5 and 1 m with respect to the MSL were taken into account since no significant changes in this part of the beach were observed and the relationship can be considered as linear (Fig. 1b, gray area). Additionally, to avoid problems due to the wave set-up, only time-stacks where incident $H_s < 2.5\ m$ were considered. A total of 184 time-stack data sets, including the 56 where the topography was available, were used to assess the spectral parameters (spectral periods and frequency spread). Incident wave conditions were quite diverse, with wave heights H_s ranging from 0.40 to 2.40 m, and incident peak periods T_p ranging from 3 to 16 s.

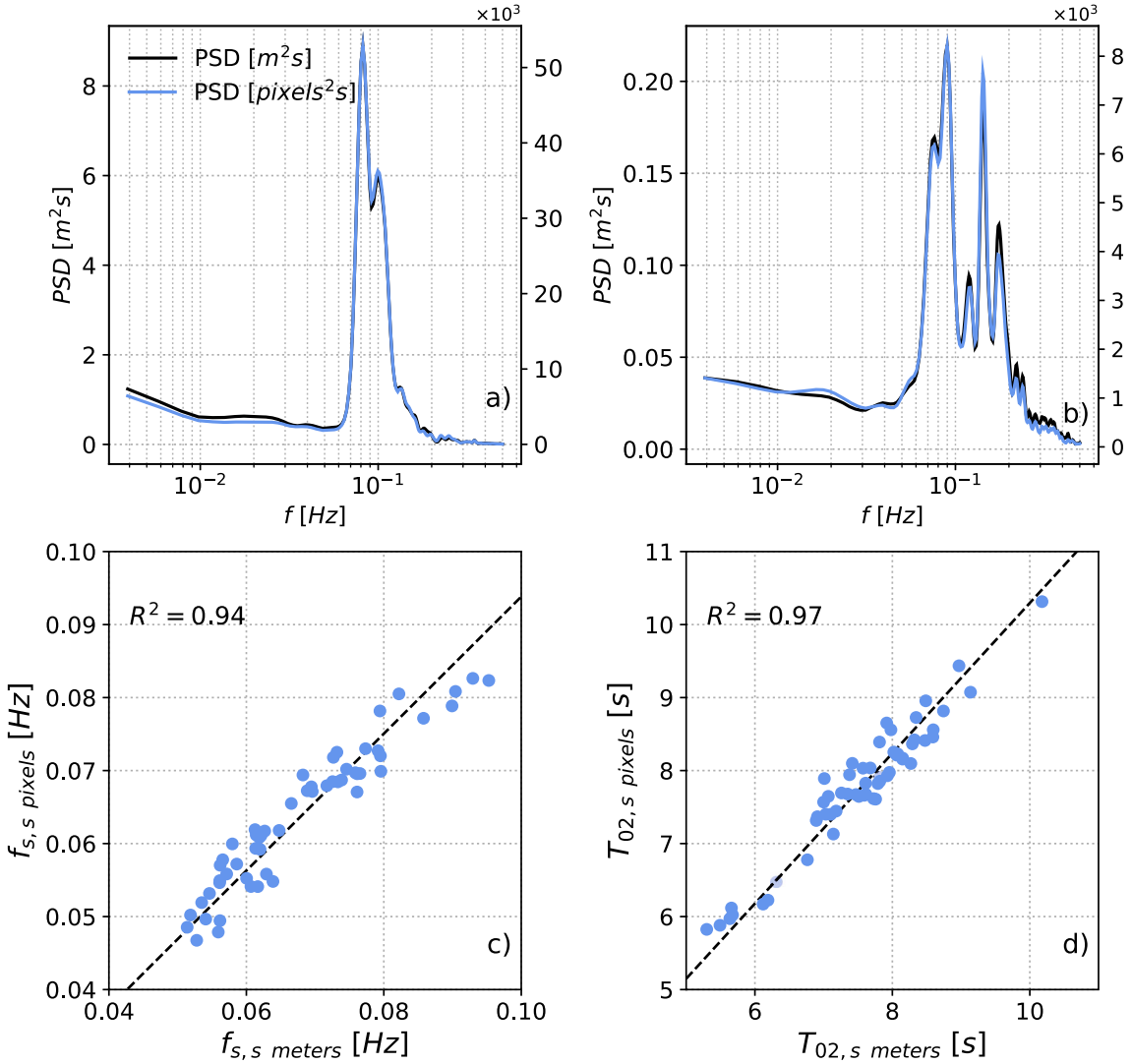

Fig. 3 **a** Spectra of the swash time-series converted to meters, i.e., vertical elevation (black line, left axis) and swash spectra of the horizontal swash excursion in pixels (blue line, right axis) on September 30, 2014. **b** Same as **a** on June 10, 2015. **c** Linear fit between $f_{s,s}$, calculated from the time-series in pixels, and $f_{s,s}$, calculated from the time-series after conversion to vertical elevation in meters. **d** Same as **c** for the mean swash period $T_{02,\,s}$

Results

Prediction of swash frequency spread $f_{s,\,s}$

For distinct periods, different run-up characteristics may be observed even when the incident bulk wave parameters (e.g., H_s, T_p) are similar. As an example, Fig. 2 (middle panels) shows a different spectral signature for incident waves and those in the swash zone. On Sep 30th, the incident wave spectrum was a bimodal spectrum, transforming into a narrow spectrum in the swash zone $f_{s,\,s} = 0.05$ Hz. Conversely, on June 10, 2015, energy is broadly distributed in both spectra (incident and swash). As expected, a direct linear relationship between the incident frequency spread f_s and swash frequency spread $f_{s,\,s}$ cannot be derived ($R^2 = 0.01$, not shown).

It was observed that the transformation of f_s from the wave buoy to the swash zone seems to be dominated by wave breaking, which may be related to the wave steepness $^{H_s}/_{L}$. we investigate the relationship between swash frequency spread $f_{s,s}$ and incident wave characteristics, we find that:

$$f_{s,s} \sim \frac{c_1}{\left(\frac{H_s}{L}\right)^{1/4} f_s T^2} \tag{1}$$

where c_1 is a dimensionless constant and f_s is the frequency spread of the incident wave spectrum. Equation 1 is inspired by a parameter for swash-swash interaction introduced by Brocchini and Baldock (2008). Figure 4 illustrates the results obtained by (1) with the 184 datasets under a variety of incident conditions. As can be seen from Fig. 4, the goodness of

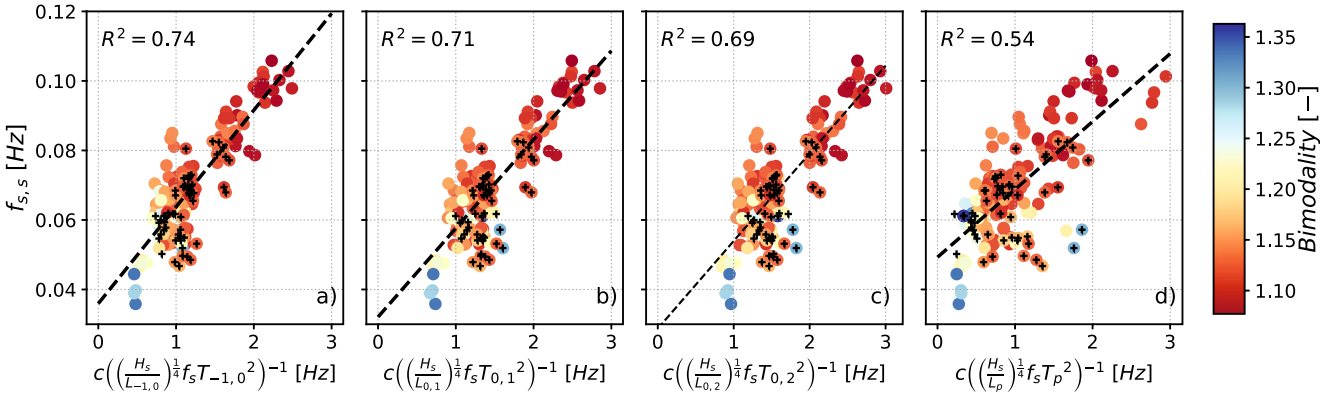

Fig. 4 Measured swash frequency spread $f_{s,s}$ vs swash frequency spread parameterization (Eq. 1), based on incident wave conditions using different definitions of wave periods **a** $T_{-1,0}$; **b** $T_{1,0}$; **c** $T_{2,0}$, **d** T_p. Crosses represent the 56 time-series where topography was available (data in meters). Colors represent the degree of bimodality of the sea state, with values >~1.2 representing bimodal spectra

fit highly depends on the selection of the wave period.

Prediction of vertical swash excursion

An exemplary broad swash spectrum ($f_{s,s} = 0.09$ Hz) is characterized by shorter and irregular swash excursions (Fig. 2b, upper and bottom panels), in contrast to longer and more organized swash excursions (Fig. 2a) for a narrow swash spectrum ($f_{s,s} = 0.05$ Hz). It is important to point out that the tidal stage and commonly used incident wave bulk parameters such as T_p and H_s are similar in both cases. However, parameters like T_p may not be appropriate to describe the sea state under bimodal conditions like those observed in September 2014.

The data shows an inverse linear relationship between frequency spread of the swash spectrum $f_{s,s}$ and swash excursion (Fig. 5). The swash excursion S on September 30th (red triangle Fig. 5a) was about 4 times larger than the swash excursion on June 10th (red cross, Fig. 5a). Both incident spectra were broad with an incident frequency spread of $f_s = 0.11$ Hz and 0.09 Hz, respectively. However, swash frequency spread in September was nearly half of the incident frequency spread, while frequency spread in June remained almost constant. Similar behavior was observed qualitatively with the horizontal swash excursion (in pixels) using the entire dataset (Fig. 5b). In the latter case, the values of swash excursion are influenced by the missing correction for topography.

The swash excursion S scales well with $f_{s,s}$ ($R^2 = 0.51$) and $f_{s,s}$ was well parameterized by incident wave characteristics (Eq. 1 and Fig. 4). Thus, a predictor for total swash excursion based on the inverse relationship found with the swash frequency spread $f_{s,s}$ (Fig. 5) can be defined by replacing $f_{s,s}$ by Eq. 1 and multiplying by $\frac{L}{T}$:

$$S = c_2 \left(\frac{H_s}{L}\right)^{1/4} f_s T L \tag{2}$$

As in Eq. 1, c_2 is a dimensionless constant. As the inclusion of the beach slope β may improve the prediction, c_2 may be a

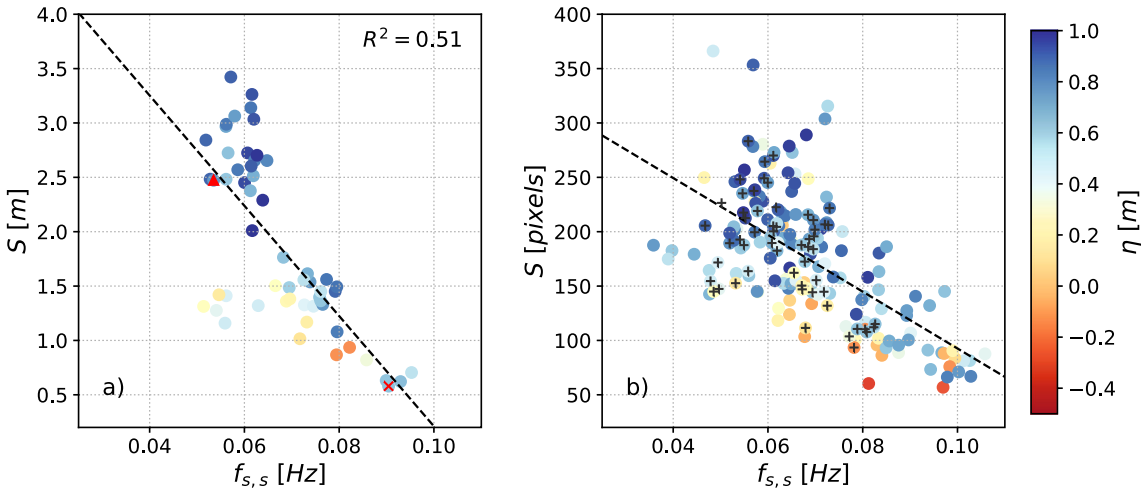

Fig. 5 **a** Swash excursion (S) in meters (56 points) vs swash frequency spread ($f_{s,s}$). The red triangle shows data on September 30, 2014 at 17:30 (Fig. 2a) and the red cross shows data on June 10, 2015 at 18:30 (Fig. 2b). **b** Same as **a** with swash excursion in pixel coordinates (184 points). Crosses indicate the 56 points shown in panel a. Dashed lines in both panels represent the best linear fit. Colors represent the tidal stage (η)

function of the beach slope $c_2 = f(\beta)$ if it is known. Notice that Eq. 2 can be also written in terms of wave period or wavelength only. However, for simplicity and to keep the structure of Eq. 1, it is expressed in terms of T and L.

The total swash excursion was predicted using Eq. 2 with $c_2 = \frac{c}{\beta}$ and evaluated for different incident wave period approximations (Fig. 6a). In addition, the influence of different variables on the predicted total swash is shown in Fig. 6b–d. The importance of the right selection of wave period is obvious. Similar to the prediction of swash frequency spread (Fig. 4), the best fit was obtained when $T_{-1,0}$ was used, reducing the scatter in the predictions even for bi-modal incident spectra (blue colors). Conversely, predictions where the peak period T_p was used displayed very low performance, underestimating S when bimodality was low and vice-versa (color coding). No significant differences were noted between the predictions with $T_{0,1}$ and $T_{0,2}$.The inclusion of the beach slope β improved the predictions (Fig. 6a, b) and, to a lesser extent, the incident frequency spread (Fig. 6a, c). The intercept in the linear regressions was forced to zero in order to avoid non-physical results in the swash predictions.

The performance of the new parameterization (Eq. 2) was compared to previous formulae by Stockdon et al. (2006) and Passarella et al. (2018), referred to hereafter as S06 and P18, respectively. Equations are provided in Appendix A. To be consistent with the original publications, incident wave conditions are represented by peak periods. Additionally, two independent datasets, Duck 1982 (Holman 1986) and Duck 1994 (Holland and Holman 1996) were used to test Eq. 2. Both study sites exhibit intermediate to reflective conditions and the presence of waves with long periods. More information about the waves and beach parameters can be found in Table 1, Stockdon et al. (2006) and Passarella et al. (2018).

Figure 7a shows the results of S06 and P18 for the Sylt dataset. Both equations were applied using T_p, and as can be seen, they are highly influenced by bimodality (color bar). S06 underestimates the predictions, with larger errors when bimodality is higher. Note that despite the high R^2 for P18, the skill of the formulation is not well as the correlation coefficient was negative ($r = -0.85$). As can be expected for the inverse relationship displayed in Fig. 7a, total swash excursion is underestimated when bimodal spectra are present (bimodality $>\sim 1.2$) and overestimated when there is no bimodality (red dots). In general, bi-modal sea states in Sylt were related to sea-states with larger values of T_p, i.e., energy concentrated in the swell band. Even without including the beach slope and using $T_{-1,0}$, Eq. 2 performed better than S06 and P18. Interestingly, no improvements were observed when $T_{-1,0}$ was used in the S06 and P18 formulae (not shown).

Similar behavior was noticed for the Duck 1982 and Duck 1994 datasets (data on bimodality could not be derived from the database). For large peak periods (blue dots), P18 underestimates the total swash excursion while for low peak periods the prediction is too high, especially for Duck 1994 (Fig. 7c). Equation 2 performed well when applied to the Duck datasets, despite the fact that the peak period T_p was used instead of $T_{-1,0}$. The beach slope was not used because including this parameter did not demonstrate any improvement. Coefficient c was similar for the Duck datasets.

Prediction of the mean swash period $T_{02,s}$

Sylt swash data revealed a strong inverse correlation ($R^2 = 0.80$) between the swash frequency spread $f_{s,s}$ and the mean swash period $T_{02,s}$ (Fig. 8a). Surprisingly, this relationship was not observed with $T_{-1,0,s}$ which showed better representation of the incident wave spectra. Therefore, calculations for the mean swash period $T_{02,s}$ were assessed using the mean incident period T_{02}. Based on the inverse relationship between $f_{s,s}$ and $T_{02,s}$ and using Eq. 1, the mean swash period may be predicted from incident parameters with:

$$T_{02,s} = c\left(\frac{H_0}{L_{02}}\right)^{1/4} f_s\, T_{02}^2 \tag{3}$$

Equation 3 resulted in a good correlation ($R^2 = 0.69$, Fig. 8b).

Discussion

Studies on beach swash spectra have found that the energy saturation slopes due to breaking of the short waves are proportional to f^{-4} (intermediate-reflective beaches) or f^{-3} (dissipative beaches) (Guza and Thornton 1982; Guedes et al. 2013; Ruju et al. 2013; Hughes et al. 2014). Further spectral shape characteristics such as Q_p, ν, ε, or f_s that describe energy distribution, i.e., narrow or broad spectra, which are commonly used to describe deep water waves, have been neglected in swash studies so far.

This study has shown that the frequency spread of swash spectra can be predicted from incident parameters that involve wave steepness H_0/L, the incident wave period T and the frequency spread f_s of the incident spectrum. Regarding f_s, we observed that despite there being no clear relationship between $f_{s,s}$ and f_s, the inclusion of this parameter in Eq. 1 improved the ability of the proposed formulae to predict $f_{s,s}$.

Commonly, swash excursion predictions are based on bulk wave parameters such as $T_p(L_p)$, H_s that can be easily acquired from wave buoys and the beach slope β. Although

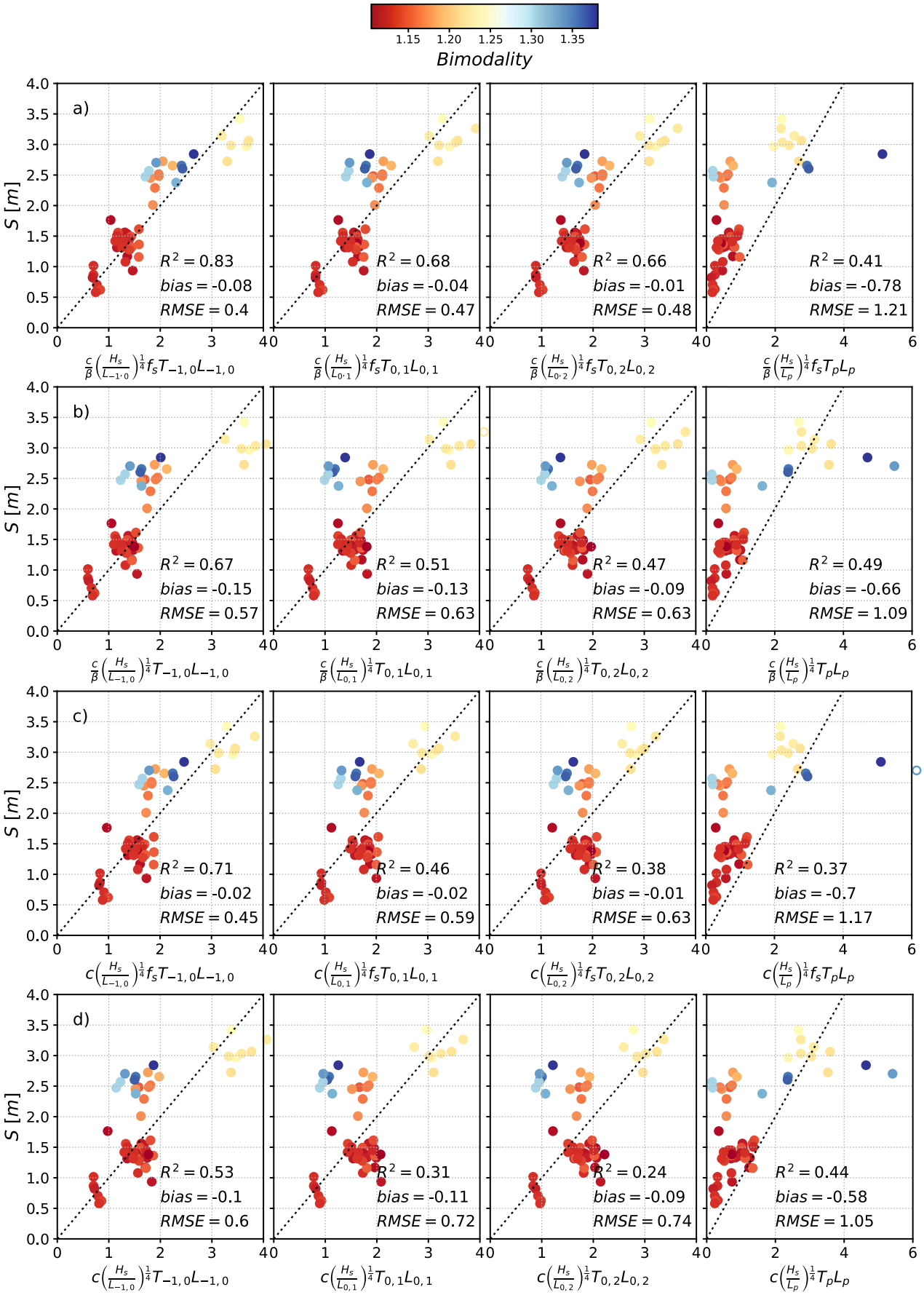
Bimodality
1.15
1.20
1.25
1.30
1.35
a)
b)
c)
d)
S [m]
$R^2 = 0.83$
bias = -0.08
RMSE = 0.4
$R^2 = 0.68$
bias = -0.04
RMSE = 0.47
$R^2 = 0.66$
bias = -0.01
RMSE = 0.48
$R^2 = 0.41$
bias = -0.78
RMSE = 1.21
$R^2 = 0.67$
bias = -0.15
RMSE = 0.57
$R^2 = 0.51$
bias = -0.13
RMSE = 0.63
$R^2 = 0.47$
bias = -0.09
RMSE = 0.63
$R^2 = 0.49$
bias = -0.66
RMSE = 1.09
$R^2 = 0.71$
bias = -0.02
RMSE = 0.45
$R^2 = 0.46$
bias = -0.02
RMSE = 0.59
$R^2 = 0.38$
bias = -0.01
RMSE = 0.63
$R^2 = 0.37$
bias = -0.7
RMSE = 1.17
$R^2 = 0.53$
bias = -0.1
RMSE = 0.6
$R^2 = 0.31$
bias = -0.11
RMSE = 0.72
$R^2 = 0.24$
bias = -0.09
RMSE = 0.74
$R^2 = 0.44$
bias = -0.58
RMSE = 1.05
$\frac{c}{\beta}\left(\frac{H_s}{L_{-1,0}}\right)^{\frac{1}{4}} f_s T_{-1,0} L_{-1,0}$
$\frac{c}{\beta}\left(\frac{H_s}{L_{0,1}}\right)^{\frac{1}{4}} f_s T_{0,1} L_{0,1}$
$\frac{c}{\beta}\left(\frac{H_s}{L_{0,2}}\right)^{\frac{1}{4}} f_s T_{0,2} L_{0,2}$
$\frac{c}{\beta}\left(\frac{H_s}{L_p}\right)^{\frac{1}{4}} f_s T_p L_p$
$\frac{c}{\beta}\left(\frac{H_s}{L_{-1,0}}\right)^{\frac{1}{4}} T_{-1,0} L_{-1,0}$
$\frac{c}{\beta}\left(\frac{H_s}{L_{0,1}}\right)^{\frac{1}{4}} T_{0,1} L_{0,1}$
$\frac{c}{\beta}\left(\frac{H_s}{L_{0,2}}\right)^{\frac{1}{4}} T_{0,2} L_{0,2}$
$\frac{c}{\beta}\left(\frac{H_s}{L_p}\right)^{\frac{1}{4}} T_p L_p$
$c\left(\frac{H_s}{L_{-1,0}}\right)^{\frac{1}{4}} f_s T_{-1,0} L_{-1,0}$
$c\left(\frac{H_s}{L_{0,1}}\right)^{\frac{1}{4}} f_s T_{0,1} L_{0,1}$
$c\left(\frac{H_s}{L_{0,2}}\right)^{\frac{1}{4}} f_s T_{0,2} L_{0,2}$
$c\left(\frac{H_s}{L_p}\right)^{\frac{1}{4}} f_s T_p L_p$
$c\left(\frac{H_s}{L_{-1,0}}\right)^{\frac{1}{4}} T_{-1,0} L_{-1,0}$
$c\left(\frac{H_s}{L_{0,1}}\right)^{\frac{1}{4}} T_{0,1} L_{0,1}$
$c\left(\frac{H_s}{L_{0,2}}\right)^{\frac{1}{4}} T_{0,2} L_{0,2}$
$c\left(\frac{H_s}{L_p}\right)^{\frac{1}{4}} T_p L_p$

◀ **Fig. 6** Measured vs predicted total swash excursion S based on Eq. 2 and subsequent simplifications: **a** Equation 2 with $c_2 = c\beta$; **b** removing the incident frequency spread f_s; **c** removing the beach slope β; **d** removing the beach slope β and the incident frequency spread f_s. Equation 2 was calculated using different incident wave periods, from left to right: $T_{-1,\,0}$, $T_{0,\,1}$, $T_{0,\,2}$, T_p. Colors represent the degree of bimodality of the sea state, with values >~1.2 representing bimodal spectra. The dotted lines represent the 45° line. Regressions were forced through the origin to avoid non-physical interpretation

parameterizations based on these parameters have performed well at predicting swash excursion in a variety of study sites (Stockdon et al. 2006; Passarella et al. 2018), they might not be applicable at locations where bimodal spectra are recurrent. Furthermore, other studies on gravel and shingle beaches that analyzed run-up parameterizations and considered bimodality (Van der Meer and Janssen 1994; Polidoro et al. 2013; Poate et al. 2016) found that the use of peak period T_p highly decreased the quality of the predictions. They concluded that other characteristic wave periods would give a better description of the incident wave conditions. Additionally, these studies also involved incident spectral shape parameters like Q_p to better describe incident wave conditions. Interestingly when S06 and P18 were applied to Sylt data using $T_{-1,\,0}$ instead of T_p, there were no improvements in the predictions. This might be explained by the fact that in both study sites (Sylt and Duck), small values of H_s may produce a large swash excursion when the wave period is large (Fig. 7, left panels). However, previous formulations imply that small values of H_s generate small swash excursions, such as the term $-\frac{T_p}{H_0}$ in P18. On the other hand, the total swash excursion is proportional to $H_s^{1/4}T^{5/2}$ in Eq. 2, which means the wave period has more weight in the parameterization than H_s. Moreover, Sylt and Duck datasets reported bi-modal spectra during measurement (Elgar et al. 1997), which, in the case of Sylt, seemed to affect the predictions. Additionally, Fig. 5a shows that there are two clusters in the data (cold and warm colors), demonstrating the influence of the tidal stage on the total swash excursion S . This has been observed previously (e.g., Guedes et al. 2011; Almar et al. 2016; Medellín et al. 2016), and it should be considered in further studies when $f_{s,\,s}$ is also considered.

It is understood that precise and timely data on beach topography are costly to obtain and rarely available. Therefore, the relevance of beach topography on the prediction of swash excursion was evaluated. As expected, considering the beach slope partly improved the predictions for the Sylt dataset. However, the selection of the right wave period parameterization was of more relevance. Moreover, the inclusion of the beach slope for the Duck dataset did not improve the predictions when we applied Eq. 2. It was noticed that common formulae such as S06 and P18 for the three study sites had less predictive ability even when the beach slope parameter was taken into account. Some authors (Ruessink et al. 1998; Guedes et al. 2011; Senechal et al. 2011) have argued that the use of a local parameter in a complex system (e.g., very different slopes in the swash and surf zones, or the presence of bars) may be misleading, and thus including beach slope does not improve the predictions. Senechal et al. (2018) found that the beach morphology in the inner surf zone has a greater influence than the beach face slope, since surf zone morphology modifies the incident wave patterns over a short cross-shore distance. Our results agree with this observation.

The data revealed a strong inverse relationship between the swash frequency spread $f_{s,\,s}$ and mean swash period $T_{02,\,s}$ (Fig. 8). This may also be the case in the offshore spectra, where low frequency swell is often narrow in frequency and direction whereas high frequency seas typically have broad sprectra (Guza and Feddersen 2012). However, we did not observe this relationship between incident frequency spread f_s and the different wave periods of the incident spectra due to the scatter caused by the bi-modal spectra (Fig. not shown). It is likely that due to dissipation of the shorter waves, bi-modal incident spectra become unimodal and narrower, allowing the inverse relationship between $f_{s,\,s}$ and $T_{02,\,s}$ to be identified. Based on Eq. 3, $T_{02,\,s}$ had a greater predictive ability than other correlations found with incident wave periods (T_p, T_{02}). This improvement in $T_{02,\,s}$ prediction may be due to Eq. 3 which involves the energy distribution of the incident wave spectra (f_s), wave dissipation through the steepness parameters H_s/L, and information on the incident wave period.

Table 1 Summary of the waves and beaches parameters used to test Eq. 2

Study site	Data points	H_s (m)	T_p(s)	β	S(m)
Sylt	56	0.4–1.46	3.6–14.3	0.11–0.14	0.6–3.4
Duck 1982	36	0.5–4.1	6.3–16.5	0.09–0.16	0.7–3
Duck 1994	52	0.7–4.1	3.8–14.8	0.06–0.1	0.8–2.9

Conclusions

This study highlights the influence of the swash frequency spread on other swash dynamics and its prediction by incident wave characteristics. We used a dataset of swash wave dynamics to analyze the energy distribution of swash spectra and its influence on other swash variables such as the total swash excursion and mean swash period. Based on our analysis we conclude that:

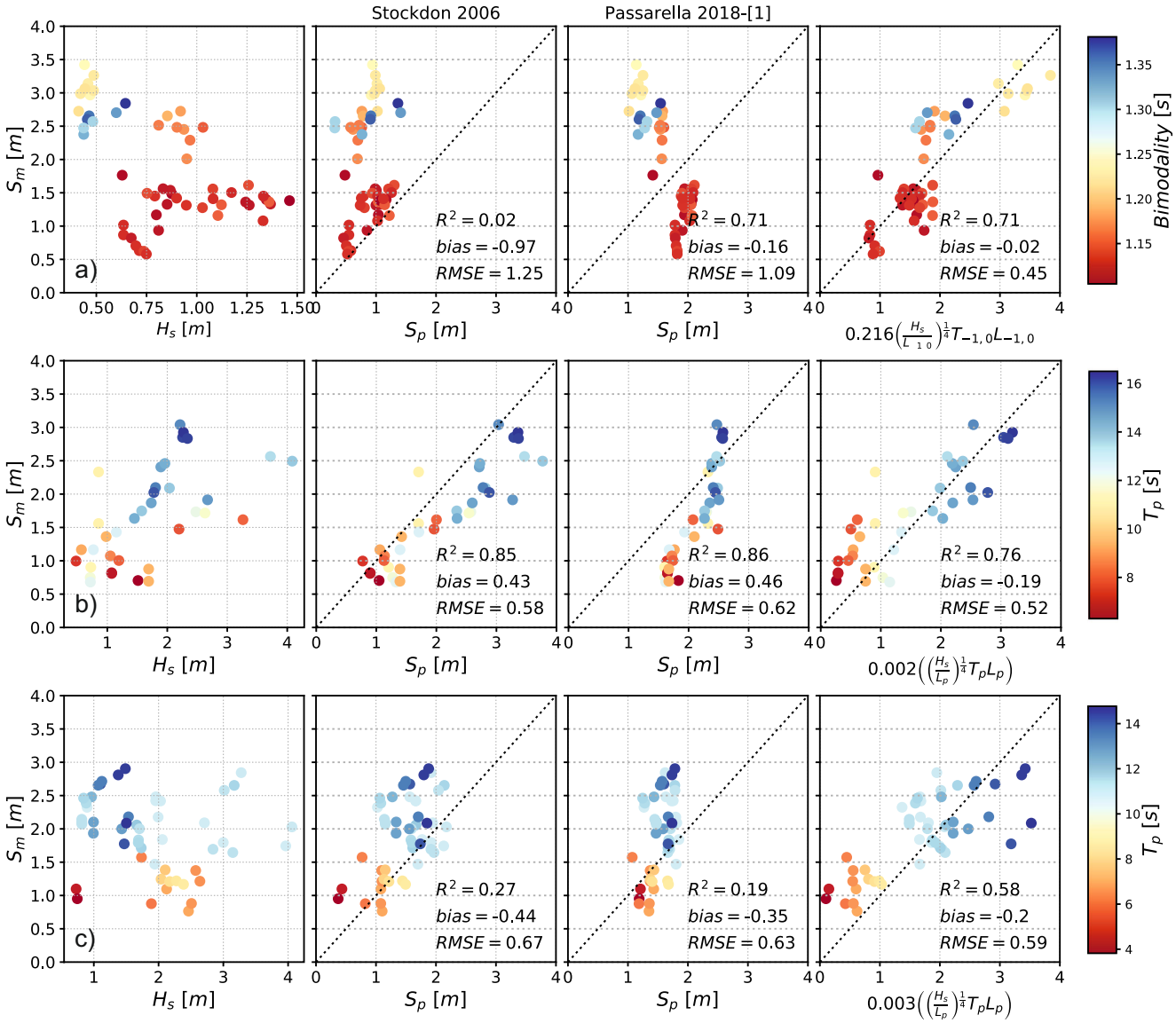

Fig. 7 From left to right: Measured total swash excursion vs H_s; swash prediction using Stockdon et al., 2006; swash prediction using Passarella et al. 2018[1] and using Eq. 2. Different datasets were used to test the equations: **a** Sylt dataset, colors represent bimodality, **b** Duck 1982 dataset, and **c** Duck 1994 dataset. Colors for **b** and **c** represent the peak period. The dotted lines represent the 45° line. Regression for Eq. 2 was forced through the origin to avoid non-physical interpretation

(1) The swash frequency spread $f_{s,\,s}$ is inversely correlated to the total swash excursion S. We found that swash spectra with low $f_{s,\,s}$ (narrow spectra) had larger swash excursions while spectra with high $f_{s,\,s}$ (broad spectra) showed shorter excursions.

(2) A formula to predict the swash frequency spread $f_{s,\,s}$ as a function of incident wave parameters is provided.

(3) Based on (1) and (2), a new formula to predict total swash excursion S by incident wave parameters is provided and tested at Sylt beach and on two independent datasets (Duck 1982 and Duck 1994) displaying better predictive ability than previous parameterizations.

(4) Although the inclusion of the beach slope may improve the total swash excursion prediction, the selection of a characteristic wave period (e. g. , $T_{-1,\,0}$, $T_{0,\,1}$, $T_{0,\,2}$, T_p) plays a more important role, especially when bi-modality is present.

To better understand swash dynamics, further studies that analyze energy distribution based on statistical parameters are needed, as have been done for deeper waters. Additionally, the influence of the frequency spread on swash dynamics needs to be tested under different environmental conditions.

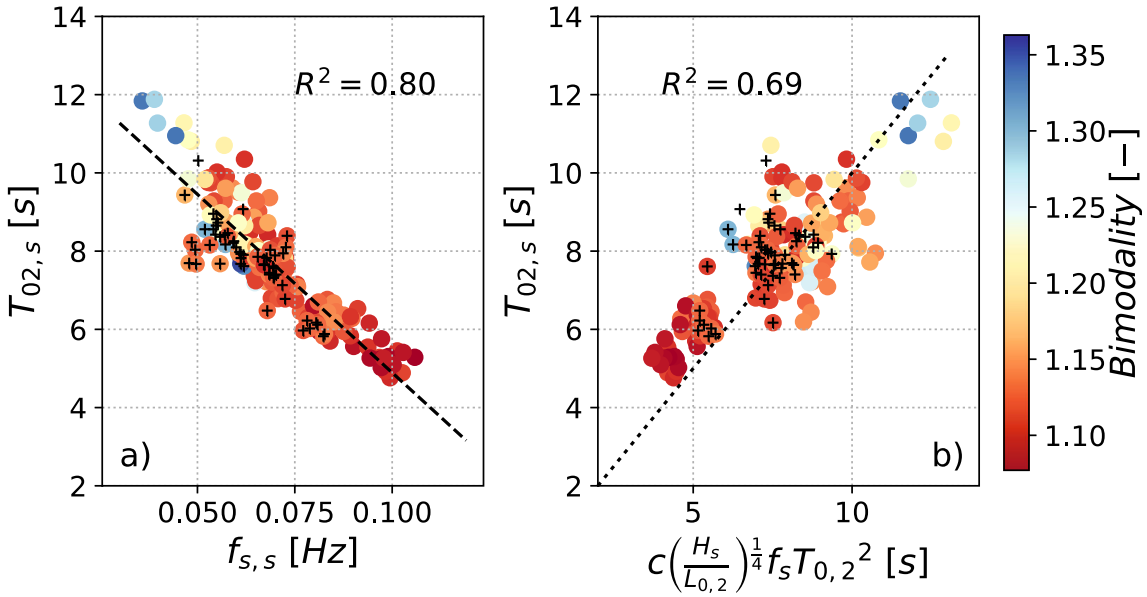

Fig. 8 **a** Relationship between $T_{02,s}$ and swash frequency spread $f_{s,s}$. The dashed line represents the best linear fit. **b** Measured mean period T_{02} vs predicted mean swash period $T_{02,s}$ based on incident wave parameters (Eq. 3). The dotted line represents the 45° line. Regression in **b** was forced through the origin to avoid non-physical interpretation. Crosses in both figures represent the data converted to meters on Sep/2014 and Jun/2015. The color bar represents bimodality with values >~ 1.2 for bimodal spectra

Acknowledgments The authors thank Helmholtz Zentrum Geesthacht (HZG) for hosting the camera system in the COSYNA framework and for the wave data which was obtained from http://codm.hzg.de/codm/. Bathymetric data was provided by Landesbetrieb für Küstenschutz, Nationalpark und Meeresschutz Schleswig-Holstein. Jennifer Montaño acknowledges the Uni-Bremen bridge scholarship for prospective PhD students. We thank Alec Torres-Freyermuth and the anonymous reviewers for valuable suggestions to improve the manuscript.

Funding information This study has been supported by the DFG-Research Center/Cluster of Excellence "The Ocean in the Earth System."

APPENDIX

Previous run-up parameterizations used in this study

Stockdon et al., (2006)

$$S = \sqrt{S_{\text{in}}^2 + S_{\text{ig}}^2}$$

Incident swash excursion is calculated as $S_{\text{in}} = 0.75\beta\sqrt{H_0 L_0}$ and swash excursion at the infragravity band is calculated as $S_{\text{ig}} = 0.06\sqrt{H_0 L_0}$.

Passarella et al. (2018)

The two equations proposed by Passarella et al. 2018 were applied in this study. However, only those obtained with P18-[1] are shown in the figures. The results obtained with P18-[2] were similar to those obtained with P18-[1].

Passarella 18-[1]:

$$S = 12.314\beta + 0.087 T_p - 0.047\frac{T_p}{H_0}$$

Passarella 18-[2]:

$$S = 146.737\beta^2 + \frac{T_p H_0^3}{5.8 + 10.595 H_0^3} - 4397.838\beta^4$$

References

Aagaard T, Holm J (1989) Digitization of wave run-up using video records. J Coast Res:547–551

Almar R, Almeida P, Blenkinsopp C, Catalan P (2016) Surf-swash interactions on a low-tide terraced beach. J Coast Res 75(sp1):348–353

Almar R, Nicolae Lerma A, Castelle B, Scott T (2018) On the influence of reflection over a rhythmic swash zone on surf zone dynamics. Ocean Dyn 68:899–909

Baldock TE, Holmes P. (1999) Simulation and prediction of swash oscillations on a steep beach. Coast eng 36(3):, 219–242

Blossier B, Bryan KR, Daly CJ, Winter C (2017) Spatial and temporal scales of shoreline morphodynamics derived from video camera observations for the island of Sylt, German Wadden Sea. Geo-Mar Lett 37(2):111–123. https://doi.org/10.1007/s00367-016-0461-7

Brocchini M, Baldock TE (2008) Recent advances in modeling swash zone dynamics: influence of surf-swash interaction on nearshore hydrodynamics and morphodynamics. Rev Geophys 46(3):1–21. https://doi.org/10.1029/2006RG000215

Bryan KR, Coco G (2010) Observations of nonlinear runup patterns on plane and rhythmic beach morphology. J Geophys Res 115(August 2009):1–16. https://doi.org/10.1029/2009JC005721

BSH (2019) https://www.bsh.de/DE/DATEN/Seegang/seegang_node.html accessed on 1.5.2019

Cartwright DE, Longuet-Higgins MS (1956). The statistical distribution of the maxima of a random function. Proceedings of the Royal Society of London. Series A. Math Phys Sci 237(1209):, 212–232

Cohn N, Ruggiero P (2016) The influence of seasonal to interannual nearshore profile variability on extreme water levels: modeling wave runup on dissipative beaches. Coast Eng 115:79–92. https://doi.org/10.1016/j.coastaleng.2016.01.006

Elgar S, Guza RT, Raubenheimer B, Herbers THC, Gallagher EL (1997) Spectral evolution of shoaling and breaking waves on a barred beach. J Geophys Res Oceans 102(C7):15797–15805

Goda Y (1970) Numerical experiments on wave statistics with spectral simulation. Rep Port Harb Res Inst 9:3–57

Gomes da Silva PG, Medina R, González M, Garnier R (2018) Infragravity swash parameterization on beaches: the role of the profile shape and the morphodynamic beach state. Coast Eng 136:41–55

Guedes RMC, Bryan KR, Coco G, Holman R (2011) The effects of tides on swash statistics on an intermediate beach. J Geophys Res 116(C4):C04008. https://doi.org/10.1029/2010JC006660

Guedes RMC, Bryan KR, Coco G (2013) Observations of wave energy fluxes and swash motions on a low-sloping, dissipative beach. J Geophys Res Oceans 118(7):3651–3669. https://doi.org/10.1002/jgrc.20267

Guza RT, Feddersen F (2012) Effect of wave frequency and directional spread on shoreline runup. Geophys Res Lett 39(11)

Guza RT, Thornton EB (1982) Swash oscillations on a natural beach. J Geophys Res Oceans 87(C1):483–491

Holland KT, Holman RA (1996) Field observations of beach cusps and swash motions. Mar Geol 134(1–2):77–93

Holman RA (1986) Extreme value statistics for wave run-up on a natural beach. Coast Eng 9(6):527–544

Holman RA, Sallenger AH Jr (1985) Setup and swash on a natural beach. J Geophys Res Oceans 90(C1):945–953

Holthuijsen LH (2008) Waves in ocean and coastal waters. Cambridge University Press https://doi.org/1-4244-1484-9/08/$25.00

Hughes MG, Aagaard T, Baldock TE, Power HE (2014) Spectral signatures for swash on reflective, intermediate and dissipative beaches. Mar Geol 355:88–97. https://doi.org/10.1016/j.margeo.2014.05.015

Longuet-Higgins MS (1983) On the joint distribution of wave periods and amplitudes in a random wave field. Proceedings of the Royal Society of London. Proc R Soc Lond A Math Phys Sci 389(1797):241–258

Masselink G, Puleo JA (2006) Swash-zone morphodynamics. Cont Shelf Res 26:661–680. https://doi.org/10.1016/j.csr.2006.01.015

Medellín G, Brinkkemper JA, Torres-Freyermuth A, Appendini CM, Mendoza ET, Salles P (2016) Run-up parameterization and beach vulnerability assessment on a barrier island: a downscaling approach. Nat Hazards Earth Syst Sci 16(1):167–180. https://doi.org/10.5194/nhess-16-167-2016

Passarella M, Goldstein EB, De Muro S, Coco G (2018) The use of genetic programming to develop a predictor of swash excursion on sandy beaches. Nat Hazards Earth Syst Sci 18(2):599–611. https://doi.org/10.5194/nhess-18-599-2018

Peláez-Zapata DS, Montoya RD, Osorio AF (2018) Numerical study of run-up oscillations over fringing reefs. J Coast Res 345:1–16. https://doi.org/10.2112/JCOASTRES-D-17-00057.1

Poate TG, McCall RT, Masselink G (2016) A new parameterisation for runup on gravel beaches. Coast Eng 117:176–190. https://doi.org/10.1016/j.coastaleng.2016.08.003

Polidoro A, Dornbusch U, Pullen T (2013). Improved maximum run-up formula for mixed beaches based on field data. In From Sea to Shore–Meeting the Challenges of the Sea: (Coasts, Marine Structures and Breakwaters 2013) (pp. 389-398). ICE Publishing.

Puleo JA, Torres-Freyermuth A (2016) The second international workshop on swash-zone processes. Coast Eng 115:1–7

Roelvink D, McCall R, Mehvar S, Nederhoff K, Dastgheib A (2018) Improving predictions of swash dynamics in XBeach: the role of groupiness and incident-band runup. Coast Eng 134:103–123. https://doi.org/10.1016/j.coastaleng.2017.07.004

Ruessink BG, Kleinhans MG, Van den Beukel PGL (1998) Observations of swash under highly dissipative conditions. J Geophys Res Oceans 103(C2):3111–3118

Ruju A, Lara JL, Michallet H, Sénéchal N, Losada IJ (2013, June). Transient swash motions on a gently sloping beach. In Proceedings Coastal Dynamics.

Sallenger AH (2000) Storm impact scale for Barrier Islands. J Coast Res 16(3):890–895. https://doi.org/10.2307/4300099

Senechal N, Coco G, Bryan KR, Holman RA (2011) Wave runup during extreme storm conditions. J Geophys Res Oceans 116(7):1–13. https://doi.org/10.1029/2010JC006819

Senechal N, Coco G, Plant N, Bryan KR, Brown J, MacMahan JHM (2018). Field Observations of Alongshore Runup Variability Under Dissipative Conditions in the Presence of a Shoreline Sandwave. J Geophys Res Oceans 123(9):, 6800–6817. https://doi.org/10.1029/2018JC014109

Stockdon HF, Holman R a, Howd P a, Sallenger AH (2006) Empirical parameterization of setup, swash, and runup. Coast Eng 53(7):573–588. https://doi.org/10.1016/j.coastaleng.2005.12.005

Van der Meer JW, Janssen JPFM (1994) Wave run-up and wave overtopping at dikes and revetments. Delft Hydraulics publication no. 485